

The effects of a comptonizing corona on the appearance of the reflection components in accreting black hole spectra

P.O. Petrucci¹, A. Merloni², A. Fabian², F. Haardt³, E. Gallo³

¹*Osservatorio Astronomico di Brera, via Brera 28, 20121 Milano, Italy*

²*Institute of Astronomy, Cambridge, UK*

³*Università dell’Insubria, Como, Italy*

arXiv:astro-ph/0108342v1 21 Aug 2001

Accepted ?. Received ?

ABSTRACT

We discuss the effects of a comptonizing corona on the appearance of the reflection components, and in particular of the reflection hump, in the X-rays spectra of accreting black holes. Indeed, in the framework of a thermal corona model, we expect that part (or even all, depending on the coronal covering factor) of the reflection features should cross the hot plasma, and thus suffer Compton scattering, before being observed. We have studied in detail the dependence of these effects on the physical (i.e. temperature and optical depth) and geometrical (i.e. inclination angle) parameters of the corona, concentrating on the slab geometry. Due to the smoothing and shifting towards high energies of the comptonized reflection hump, the main effects on the emerging spectra appear above 100 keV. We have also investigated the importance of such effects on the interpretation of the results obtained with the standard fitting procedures. We found that fitting Comptonization models, taking into account comptonized reflection, by the usual cut-off power law + uncomptonized reflection model, may lead to an underestimation of the reflection normalization and an overestimation of the high energy cut-off. We discuss and illustrate the importance of these effects by analysing recent observational results as those of the galaxy NGC 4258. We also find that the comptonizing corona can produce and/or emphasize correlations between the reflection features characteristics (like the iron line equivalent width or the covering fraction) and the X-ray spectral index similar to those recently reported in the literature. We also underline the importance of these effects when dealing with accurate spectral fitting of the X-ray background.

Key words: radiation mechanisms: thermal – X-rays: general

1 INTRODUCTION

The presence of secondary components in the spectra of Seyfert galaxies and Galactic Black Hole Candidates (GBHC), such as an iron line at ~ 6.4 keV and a reflection hump between 10 and 50 keV, superimposed on the primary X-ray continuum, is now well established observationally (Nandra & Pounds 1994). Discovered in the late eighties with the *GINGA* satellite (Matsuoka et al. 1990; Pounds et al. 1990), they are signatures of reprocessing of the primary X-ray emission in surrounding cold ($T \leq 10^5$ K) and optically thick matter accreting onto the central engine. Indeed, part ($\sim 10\%$) of the primary X-ray radiation may be Compton reflected at the gas surface, producing the observed secondary features (Bai & Ramaty 1978; Lightman & White 1988; George & Fabian 1991; Matt, Perola & Piro 1991; Magdziarz & Zdziarski 1995). The remaining incident flux is reprocessed in the UV/Soft X-ray band and is be-

lieved to form part of the UV–soft X-ray excess (the so-called UV bump) generally observed in this class of objects.

The reflections features are of great importance in testing theoretical models of the high energy emission in compact objects since they give crucial (while undirect) constraints on the geometry and on the nature of the emitting regions.

Compton scattering of the soft photons emitted by the thick matter on a population of hot thermal electrons is the best model to date for the primary high energy emission in these objects. Indeed, the so-called corona models, which assume radiative equilibrium between the thermal comptonizing plasma and the underlying cold matter (generally an accretion disk), can naturally account for the average properties of the X-ray emission of black holes accretion flows (Haardt & Maraschi 1991). It has also been shown that a

patchy geometry, where the corona is disrupted in localized blobs, appears to be in better agreement with the spectral variability and L_{UV}/L_X ratios observed for example in Seyfert galaxies (Haardt 1994; Stern et al. 1995). In the case of GBHC, like Cyg X-1, simple slab–corona models even fail to fit the high signal to noise X-ray spectra of these objects and more complex configurations are required (Gierlinski et al. 1997). The real geometry of the corona–disk system is thus relatively difficult to constrain in the framework of this class of models and the reflection features can give some important clues in this respect.

An alternative model for the high energy emission in black hole spectra consists of an advection-dominated accretion flow (ADAF) near the central engine. ADAFs are expected to occur in low mass accretion rate objects, where the hot plasma density is low enough to prevent a rapid energy transfer from protons to electrons. Most of the accretion energy is then advected into the central black hole rather than being radiated (Narayan et al. 1998, and references therein).

The amount of reflection is expected to be different in these different scenarios. For instance, in a disk–corona configuration we expect a reflection fraction of the order of unity, since the reflected disk, as seen by the hot corona, subtends a solid angle of 2π . On the other hand, in the case of a truncated disk–ADAF model, the solid angle would be smaller due to the lack of reflecting matter in the central regions. For the same reason, we expect narrower iron $K\alpha$ fluorescent lines since relativistic effects, which are stronger in the vicinity of the black hole, are negligible in the ADAF interpretation.

We thus expect the reflected spectrum to provide a strong observational test to discriminate between these distinct models and between different possible geometries. However, various effects may complicate the situation. For instance, the complex ionization pattern of the reflector can strongly mask and/or modify the reflection features in comparison to what we expect in the case of a simple neutral material or even single–zone ionization model. Done & Nayakshin (2001) and Ballantyne, Ross & Fabian (2000) have recently shown that using single–zone ionization models can severely underestimate the reflection normalization if the accretion disk is highly ionized. It can even produce an apparent correlation between the reflection normalization and the spectral photon index similar to that reported by Zdziarski et al. (1999) in a sample of Seyfert galaxies and galactic black hole candidates. The presence of a dynamic hot corona (Reynolds & Fabian 1997; Beloborodov 1999; Malzac, Beloborodov & Poutanen 2000) will also strongly modify the reflection spectrum due to the anisotropic illumination produced by relativistic motions inside the corona.

We present here another important effect which will also modify the appearance of the reflection components. Indeed, in a corona–disk configuration, we expect that part (or even all, depending on the coronal covering fraction) of the reflection features cross the comptonizing plasma before being observed. In this case, the reflected photons are also Compton scattered in the corona and the shape of the secondary

spectral components may be significantly modified as compared to the one expected when no Comptonization in the corona is taken into account.

The effects of the hot corona in modifying the reflection component have been already noted by some authors (Haardt et al. 1993b). The aim of this paper is thus to study more precisely the dependence of these effects on the physical (temperature and optical depth) and geometrical (inclination angle) parameters of the hot corona. We are also interested in the consequence for spectral analysis of real data when these effects are taken into account. We mainly focus on the slab geometry where the effects are expected to be large since the corona completely covers the reflecting material.

The paper is organized as follows. In section 2 we briefly summarize the main characteristics of the Comptonization model we used. We discuss the effects of a comptonizing corona on the reflection hump shape, varying the corona optical depth and/or temperature and for different inclination angles in section 3. In section 4, we focus on the iron line and on how the Comptonization process affects the measurement of its equivalent width. We also investigate, in section 5, the importance of these effects on the interpretation of the results obtained with the standard fitting procedures. We discuss and illustrate the importance of these effects in section 6 by analysing recent observational results as those of the galaxy NGC 4258. We also show that the comptonizing corona can produce apparent correlations between the reflection features characteristics (like the iron line equivalent width or the covering fraction) and the X-ray spectral index similar to those recently reported in the literature. We finally underline the importance of these effects when dealing with accurate spectral fitting of the X-ray background before concluding.

2 THE MODEL

We use the thermal Comptonization code of Haardt (1994, hereafter H94). This code computes the angle–dependent spectrum of the disk–corona system in a slab configuration using an iterative scattering method, where the scattering anisotropy is taken into account only up to the first scattering order. It also computes, separately, the reflection components obtained including or not the comptonization effects. They will be denoted R_{dir} and R_{comp} , respectively, in the following. The continuum will be simply called C .

The reflection component R_{dir} is computed following White, Lightman & Zdziarski (1988) and Lightman & White (1988); thus, the spectral shape of the reflected photons is averaged over angles. It is well-known that the actual shape of the reflection component does depend on the viewing angle, especially at high energy. Such angular distortion is relatively complex and is a function of the photon energy. The main effects occurs in hard X-rays and soft γ -rays bands, where the reflected spectra strongly hardens with increasing viewing angle (Hua & Lingenfelter 1992; Magdziarz & Zdziarski 1995). We have checked *a posteriori* (cf. section 3.2 and Fig. 3) that the effects produced by such angular dependence are always smaller than the one we discuss here.

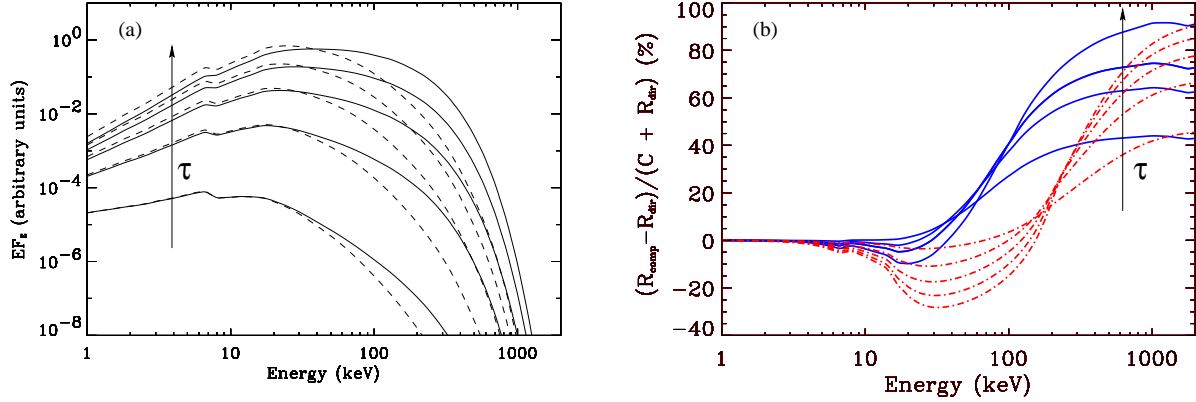


Figure 1. (a) The comptonized (solid lines) and uncomptonized (dashed lines) reflection humps, R_{comp} and R_{dir} , for different values of the coronal optical depth, the temperature being fixed to $kT_e=50$ keV. From bottom to top, $\tau=0.1, 0.3, 0.5, 0.7$ and 0.9 . (b) Deviations (in %) between the outgoing spectra. The solid line and dot-dashed lines correspond to $kT_e = 50$ keV and 350 keV respectively.

Consequently, in the rest of the paper, we will normalize the spectrum at different viewing angles by just multiplying the reflection component by the angular function

$$f(\mu) = \frac{3\mu}{4} \left[(3 - 2\mu^2 + 3\mu^4) \ln \left(1 + \frac{1}{\mu} \right) + (3\mu^2 - 1) \left(\frac{1}{2} - \mu \right) \right], \quad (1)$$

neglecting any energy dependence (see Ghisellini, Haardt & Matt 1994 for details). It is worth noting that the shape of the reflection component averaged over angles is very similar to the real shape expected with an inclination angle of 60° .

The effect of Comptonization on the reflection component will depend mainly on three physical parameters: the temperature kT_e and the vertical optical depth τ of the corona and the inclination angle i (or its cosine $\mu = \cos i$). The last two parameters may be combined to give an “effective” optical depth $\tau_\mu = \tau/\mu$, which is the line-of-sight optical depth that a photon, emitted at the surface of the disk, has to cross in order to escape from the corona without being comptonized and reach an observer at the viewing angle i .

The soft temperature of the cold matter kT_{bb} , does not play an important role in the problem we study here. In fact, in an anisotropic geometry, as the one we are dealing with, the spectrum emitted by the corona depends on such temperature because of the presence of an anisotropy break (Stern et al. 1995; Svensson 1996; Haardt, Maraschi & Ghisellini 1997; Petrucci et al. 2000). Such a break is due to the apparent reduced contribution of the first Compton scattering order, mainly emitted backward towards the disk, to the outgoing flux. The spectrum is then better approximated by a convex broken power law where the break energy depends mainly on kT_e and kT_{bb} . Changing kT_{bb} will thus modify the shape of the X-ray spectrum impinging on the cold matter and consequently the shape of the reflection components R_{dir} and R_{comp} . However, we have checked that these effects are negligible in comparison to the ones we are looking at. We will thus fix kT_{bb} to a constant value of 10 eV in the

following.

3 COMPTONIZATION EFFECTS ON THE REFLECTION HUMP SHAPE

3.1 Dependence on the physical parameters of the corona

In this section we will firstly discuss the effect of the Comptonization in the corona on the shape of the reflection component varying the optical depth and/or the temperature of the corona, but keeping fixed the viewing angle (here $\mu = 0.9$). According to thermal Comptonization theory, the temperature of the corona is directly related to the average fractional energy change that a photon undergoes per scattering, whereas τ gives an estimate of the mean number of scattering events. Both parameters play thus a major role in the Comptonization process.

3.1.1 Varying τ at fixed coronal temperature

We will first suppose here that the temperature of the corona is fixed, equal to 50 keV, while τ varies. We have plotted in Fig. 1a the reflection shapes of R_{dir} and R_{comp} (in dashed and solid line respectively) for different values of τ .

The increase of the optical depth hardens the X-ray primary spectrum, thus modifying the intrinsic shape of the reflection component. It thus explains the hardening of the uncomptonized reflection R_{dir} between $\tau=0.1$ and $\tau=0.9$. Increasing τ also magnifies the effect of the Comptonization. The larger τ , the larger the probability of a photon to be comptonized. In this process the reflected photons are shifted towards higher energies and an increasing deviation between R_{dir} and R_{comp} is seen, at energies below and above $\sim kT_e = 50$ keV, for increasing τ .

The optical depth of the corona also controls the relative intensity of the different Compton scattering orders. The larger τ , the higher the intensity of the different orders

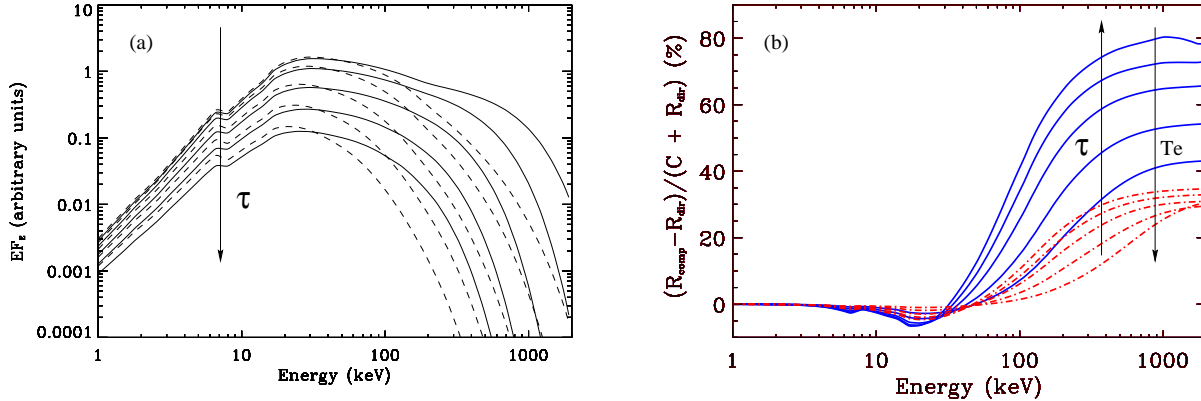


Figure 2. (a) As in Fig. 1a, but for a constant Compton parameter y equal to 0.6, i.e. consistent with a slab corona in radiative equilibrium above a passive accretion disk. From bottom to top $\tau=0.1, 0.2, 0.35, 0.5$ and 0.64 and $kT_e=240, 150, 90, 65$ and 50 keV. (b) As in Fig. 1b but for a constant Compton parameter y equal to 0.6 (solid line) and 2 (dot-dashed lines). The latter case is consistent with a hemispherical corona in radiative equilibrium above a passive accretion disk.

producing a hardening of the comptonized shape at high energy (above ~ 10 –30 keV) as observed in Fig. 1a.

To estimate quantitatively these effects on the total outgoing spectrum, we have plotted in Fig. 1b (solid lines) the deviations (in %) between the total spectrum ($C + R_{\text{comp}}$), expected if all the reflected photons cross the comptonizing corona before being observed, and the total one ($C + R_{\text{dir}}$) predicted when the Comptonization of the reflection hump is not taken into account. The most important effects (variations of $> 50\%$) occur at very high energies (above 100 keV). They are due to the hardening of R_{comp} for large optical depths. For the larger optical depth case considered ($\tau = 0.9$), a factor of ~ 2 is expected near 1 MeV. At these energies, R_{comp} tends to have the same shape as the primary continuum and the fractional deviations between the two spectra attain a maximum.

The Comptonization produces also smaller ($< 10\%$) differences between R_{dir} and R_{comp} near 10 keV. The larger one is still produced in the high optical depth case, as expected. It is worth noting that the X-ray detectors are generally well sensitive in the 10–20 keV energy range, which can help constraining the degree of Comptonization.

Also plotted in Fig. 1b are the results obtained for a coronal temperature of 350 keV (dot-dashed lines). We can still observe differences between R_{dir} and R_{comp} below and above $\sim kT_e$. However, such deviations are larger than in the previous case, at least at low energy (below 100 keV), since the average fractional energy change of a scattering photon increases with kT_e . These deviations reach $\sim 40\%$ near 20–30 keV for $\tau = 0.9$. Above 100 keV, they roughly behave as in the small temperature case.

3.1.2 Varying τ and T_e at fixed Compton parameter

In the case of a disk–corona system, such as the one we are dealing with, we expect the comptonizing region and the source of soft photons to be *coupled*, as the optically thick disk necessarily reprocesses and re-emits part of the

comptonized flux as soft photons which are the seeds for Comptonization. In this case, the system can only be in equilibrium if the temperature and optical depth satisfy a precise relation (Haardt & Maraschi 1991). That in turn corresponds to roughly constant Compton y parameters, defined as:

$$y = 4 \left(\frac{kT_e}{m_e c^2} \right) \left[1 + 4 \left(\frac{kT_e}{m_e c^2} \right) \right] \tau (1 + \tau), \quad (2)$$

which is about 0.6 in a slab geometry when all the accretion power is released in the corona (Haardt & Maraschi 1993a; Stern et al. 1995; Svensson 1996).

In the case of a constant Compton parameter, changes in τ will be necessarily accompanied by changes in kT_e , namely a larger optical depth will require a smaller coronal temperature. This results in three effects: first, the photon index of the primary continuum correlates with τ (Haardt, Maraschi & Ghisellini 1997), whereas these two parameters are anti-correlated if the temperature is kept fixed (cf. section 3.1.1). Second, the variation of the coronal temperature modifies the high energy cut-off of the primary continuum, which scales roughly as $2kT_e$. Consequently, it slightly modifies the high energy part of the reflection component R_{dir} . Finally, the change of kT_e modifies the mean photon energy gain per scattering.

These different effects produce a hardening of R_{comp} at high energy when τ decreases as can be seen in Fig. 2a. This behavior is thus the opposite of what we obtained when the temperature is fixed. However, as shown in Fig. 2b (solid lines), the deviations between the outgoing spectra closely resemble those shown in Fig. 1b, becoming larger for larger optical depth (i.e. smaller temperature) and reaching a plateau at high energies (above 200 keV). For comparison, we have also plotted the deviation curves obtained in the case of a hemispherical geometry in radiative equilibrium (dot-dashed lines). In this case, the Compton parameter is of the order of 2 (if all the accretion power is released in the corona, see Stern et al. 1995). We see that the deviations are smaller (by about a factor of 2) than in the slab case. This is simply due to the fact that in hemispherical geometry,

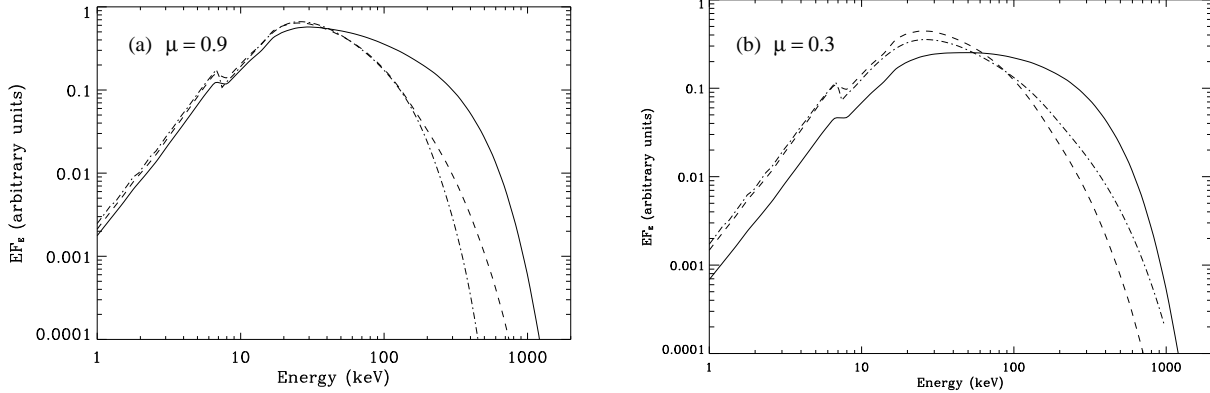


Figure 3. Plots of R_{comp} (solid line), R_{dir} (dashed line) and R_{pexrav} (dot-dashed line) at two different viewing angles: (a) $\mu=0.9$ and (b) $\mu=0.3$.

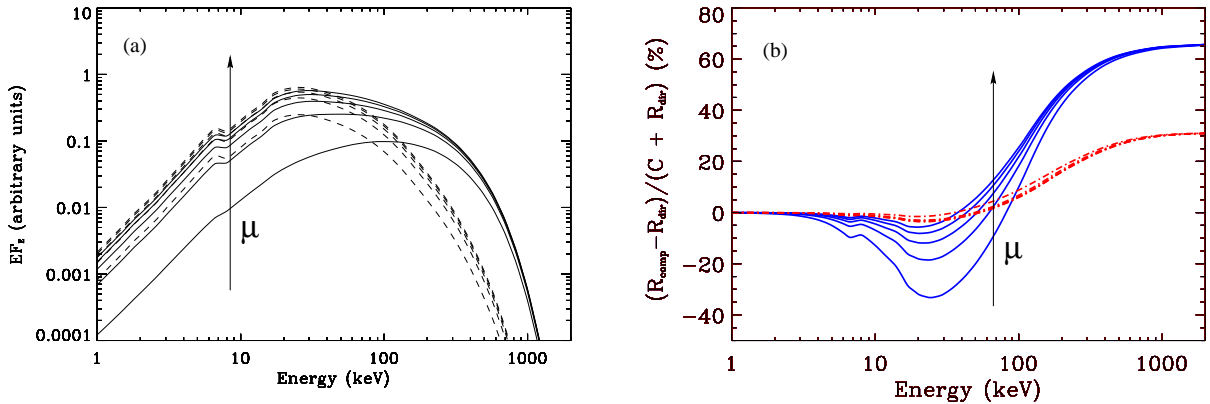


Figure 4. (a) The comptonized (solid lines) and uncomptonized (dashed lines) reflection humps, R_{comp} and R_{dir} , for different viewing angle. From bottom to top $\mu=0.1, 0.3, 0.5, 0.7$ and 0.9 . The optical depth and temperature of the corona are fixed to 0.35 and 90 keV respectively. (b) Deviations (in %) between the outgoing spectra. In dot-dashes line the case of an hemispherical corona with $\tau=0.35$ and $kT_e=200$ keV.

the corona does not cover all the cold disk. Consequently, only a part of the reflected photons have to cross the comptonizing plasma before being observed, reducing the effects of Comptonization.

3.2 Dependence on the inclination angle

In this section we fix the temperature and optical depth of the corona to 90 keV and 0.35 respectively. Those values correspond to a Compton parameter y close to 0.6 , i.e. consistent with a slab corona in radiative equilibrium above a passive accretion disk (cf. previous section). We focus here on the dependence of the Comptonization effects on the system viewing angle.

As already mentioned in the introduction, the actual shape of the reflection hump depends on μ in a relatively complex manner which is a function of the photon energy. We recall that this angular dependence is neglected in our computation of R_{dir} , whose shape is constant and corresponds to the angular averaged one. We have plotted in Figs. 3a and 3b the reflection component R_{dir} , computed

by our code (dashed line), and the one computed following Magdziarz & Zdziarski (1995), obtained with the PEXRAV model of XSPEC, and noted R_{pexrav} (dot-dashed line), for two different inclination angles $\mu = 0.9$ (Fig. 3a) and $\mu = 0.3$ (Fig. 3b). R_{pexrav} is computed using angle dependent Green functions and takes properly into account the angular distortion of the Compton reflection. The continuum assumed to compute R_{pexrav} corresponds to the best cut-off power law fit of the spectrum emitted by our slab corona model, that is a photon index $\Gamma \simeq 2.2$ and a high energy cut-off $E_c \simeq 250$ keV. The primary spectra impinging on the disk are thus roughly similar in the two models. We see in Fig. 3a and 3b that the main differences between R_{dir} and R_{pexrav} appears above 10 keV. R_{pexrav} also hardens for increasing i (i.e. decreasing μ). For comparison, we have also plotted on these figures the comptonized reflection R_{comp} computed with our model. It is evident that the effects of the Comptonization on the reflection hump are generally more important than the intrinsic angular ones, especially at high energies. Therefore, in the following we will simply use Eq. (1) to rescale the amplitude of the reflection component as a function of

Keeping in mind the limitations of the above approximation, we have plotted in Fig. 4a, the different shapes of R_{comp} and R_{dir} for different values of the viewing angles. Because an increase of i will correspond to an increase of the effective optical depth τ_μ , we expect to observe, for increasing i , the same effects we observed for increasing τ (cf. section 3.1). However, the main difference is that now the shape of the primary spectrum impinging on the accretion disk is constant.

The differences between R_{comp} and R_{dir} are relatively strong (cf. Fig. 4a). In our case, τ_μ can easily reach values of the order of 2 or 3 for large inclination. It thus results in large mean photon energy shifts and hardening of R_{comp} at high energy. The deviations between R_{dir} and R_{comp} are reported in Fig. 4b. They may be as large as $\sim 30\%$ in the 10–50 keV range for $\mu=0.1$ whereas they are of the order of a few for nearly face-on configuration.

Above 100 keV the different shapes overlap near $2kT_e$ the larger energy that a photon may reach by Comptonization in the corona. It is worth noting that this overlapping is a direct consequence of our treatment of the angular dependence of the reflection hump. Actually, the reflection shapes for different inclination angles would be different especially at high energies. The deviations would however not strongly depend on the real reflection shape and we see that they are of the order of 60% near 300 keV for a slab geometry. They reach only 30% for an hemispherical corona since the Comptonization effects are less important in this case (cf. section 3.1.2).

We note however that the Comptonization effects beyond ~ 100 keV may not be easily detected. Firstly because the high energy instruments are generally not very sensitive beyond ~ 100 keV and thus prevent any good constrains on the spectral shape. Secondly, any deviations from the ideal case studied here like, for instance, a stratified temperature corona, may distort the derived reflected shape, especially at high energy, and complicate the spectral analysis. The effects at lower energy (near ~ 20 keV where the instrumental sensitivity is very good) would certainly be more relevant for any estimation of the comptonization effects.

4 COMPTONIZATION EFFECTS ON THE IRON LINE

The equivalent width (EW) of the fluorescent Fe K α line produced by cold matter surrounding the hot corona depends on different parameters, as the elemental abundance of the reflecting matter, its inclination angle as seen by the observer, and the ionization state of the reflecting surface layers (see Fabian et al. 2000 for a review). It also depends on the geometry of the corona + cold matter configuration (i.e. on the solid angle subtended by the cold matter as seen by the X-ray source). The Comptonization of the iron line is another process which may affect the measurement of this EW as pointed by Haardt et al. (1993b) and discuss by Matt

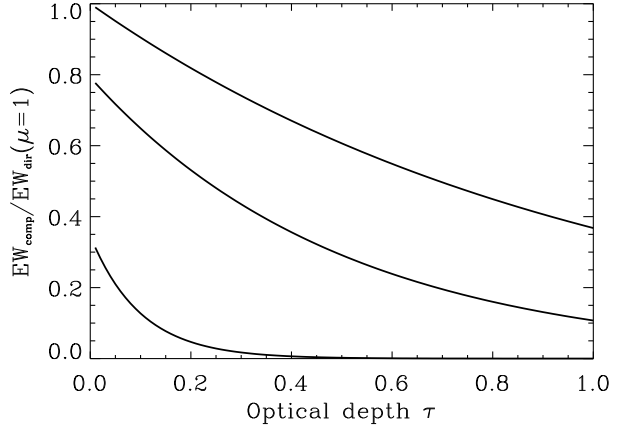


Figure 5. Reduced equivalent width $EW_{\text{comp}}(\mu)/EW_{\text{dir}}(\mu=1)$ of the comptonized iron line in function of the optical depth of the corona for different inclination angles. From top to bottom $\mu = 1, 0.5$ and 0.1

et al. (1997). We try to quantify a bit more this effect here.

Assuming a slab corona geometry above an accretion disk of neutral matter and solar abundance, the dependence of the EW on μ can be approximated by the simple formula:

$$\begin{aligned} EW_{\text{comp}}(\mu) &= \frac{EW_{\text{dir}}(\mu=1)}{\ln 2} \mu \ln \left(1 + \frac{1}{\mu} \right) e^{-\tau_\mu} \quad (3) \\ &= EW_{\text{dir}}(\mu) e^{-\tau_\mu}. \end{aligned}$$

The term before the exponential is an approximated formula, given by Ghisellini et al. (1994), of the angular dependence of the equivalent width due to limb darkening, $EW_{\text{dir}}(\mu=1)$ corresponding to the face-on EW of the uncomptonized line. The exponential term $e^{-\tau_\mu}$ gives the probability of a line photon to cross the corona and reach an observer at the viewing angle i without being comptonized. The comptonized ones will be scattered around in the underlying continuum and will not contribute to the line flux anymore.

We have plotted in Fig. 5 the reduced equivalent width $EW_{\text{comp}}(\mu)/EW_{\text{dir}}(\mu=1)$ as a function of the optical depth of the corona and for different viewing angles. We see that the effects of Comptonization are very strong, especially at large inclination angles. For $\mu = 0.9$ the EW is reduced by a factor ~ 3 when τ varies between 0 and 1 whereas it becomes rapidly negligible for $\tau > 0.5$ if $\mu = 0.1$. We thus expect these modifications of the Iron line EW to be a lot more observable than the spectral changes of the reflection hump detailed in section 3

5 APPLICATION TO FITTING PROCEDURES

In section 3 we have discussed, in an admittedly qualitative way, the changes in the observable reflection hump due to the presence of a comptonizing corona above the cold reflector (the accretion disc). Here we will try to give a more quantitative estimate of such an effect. To do so, we have to

rely on some simple and straightforward measure of the reflection component, and compare such a measure in the two cases of a bare disc and of a disc engulfed in a hot optically thin corona.

The most widely used model to fit the hard X-ray continuum of Seyfert galaxies and GBHC comprises a cut-off power law and an uncomptonized reflection (the so-called PEXRAV model of XSPEC, Magdziarz & Zdziarski 1995). This model is known to be a poor approximation to the true Compton continuum since it does not reproduce the (possible) anisotropy break (cf. section 2) and may give (mainly for high, i.e. larger than 1, optical depth) a poor modelisation of the high energy cut-off shape. However, it can help to quantify the effects of a comptonizing corona on the appearance of the hard X-ray continuum. For this purpose we have proceeded in the following way. We have first created two sets of simulated spectra using the thermal Comptonization code of H94 in a slab geometry. In the first set we have properly taken into account the Comptonization of the secondary components in the corona, while in the second one we have neglected such effect. Then we have fitted our simulated spectra between 1 and 500 keV with the PEXRAV model. We have assumed different viewing angles and different values for coronal temperature and optical depth, chosen as to keep $y = 0.6$. For every simulated spectrum, our fitting procedure gives the best fit value of the spectral index, the high energy cut-off and of the reflection fraction. We will denote R_1 and $E_{c,1}$, respectively, the value of the reflection fraction and of the high energy cut-off obtained for the comptonized model, and R_2 and $E_{c,2}$ the ones obtained for the uncomptonized case. The ratio R_1/R_2 and $E_{c,2}/E_{c,1}$ can then help to quantitatively estimate the modifications of the best fit parameter values due to the comptonization effects.

In Fig. 6 we show the ratio R_1/R_2 as a function of the optical depth and for different viewing angles i . As expected, due to the smoothing effect of the comptonizing corona on the reflection shape, R_1 is always smaller than R_2 , because the fitting procedure needs smaller reflection normalization to fit the comptonized component. Furthermore, their ratio decreases with increasing i and/or optical depth in the corona. This is in agreement with the results of section 3.

The shifting of the reflection hump R_{comp} towards high energies (as discussed in section 3) as a consequence of the Comptonization, modifies also the high energy part of the spectra and the estimate of the high energy cut-off so that it is always larger for the comptonized case. The amount of such shift depends on the temperature and optical depth of the corona (cf. Fig. 2a) and the higher the temperature, the higher the energy of the scattered photons. At the same time, however, in our simulations, higher coronal temperature corresponding to lower optical depth, the effect of the anisotropy break has to be taken into account. When trying to fit the curved spectrum with a cut-off power-law, we obtain a lower value spectral index and, consequently, a lower cut-off energy. The net result is shown in Fig. 7, where we have plotted the ratio $E_{c,2}/E_{c,1}$ of the measured cut-off energies as functions of the optical depth for different viewing angles. The ratio has a minimum for $\tau \simeq 0.4$. At the highest

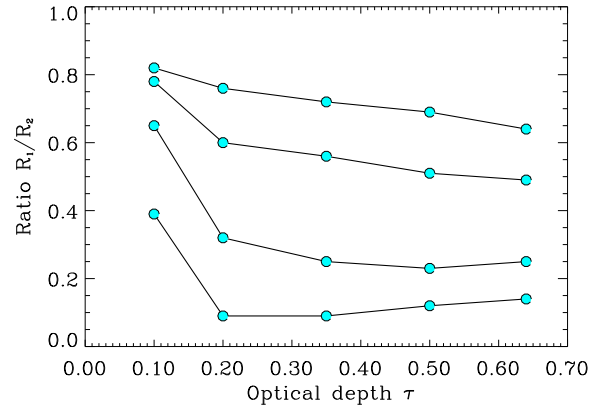


Figure 6. Ratio R_1/R_2 versus the coronal optical depth for different viewing angles but keeping the Compton parameter y equal to 0.6. From top to bottom $\mu=0.9, 0.5, 0.2$ and 0.1

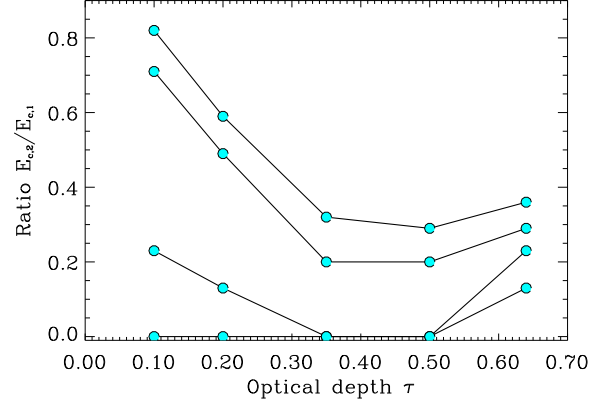


Figure 7. Ratio $E_{c,2}/E_{c,1}$ versus the coronal optical depth, for different values of μ . From top to bottom $\mu=0.9, 0.5, 0.2$ and 0.1

inclination angle ($\mu=0.1-0.2$) we are unable to constrain the high energy cut-off in the comptonized case $E_{c,1}$, below 500 keV, so we report for the ratio $E_{c,2}/E_{c,1}=0$.

The main qualitative conclusion of this section is that fitting Comptonization models that take properly into account the comptonized reflection by the usual cut-off power law + uncomptonized reflection leads to an underestimation of the reflection normalization and also to an overestimation of the high energy cut-off. Quantitatively, these effects will of course strongly depend on the quality of the data, especially at high energy (above 100 keV).

6 OBSERVATIONAL CONSEQUENCES

6.1 The case of NGC 4258

From the X-ray point of view, the nearby bright galaxy NGC 4258 possesses the general characteristic of the Seyfert class, that is: a power law primary continuum with a photon index $\Gamma \simeq 2$, a relatively large amplitude variability in the 3-10 keV band on time scales of a few tens of thousands

of seconds and smaller ones ($\sim 20\%$) on time scales of the order of an hour (Reynolds et al. 2000, hereafter R00; Fiore et al. 2001, hereafter F01) and the presence of a (narrow) iron line near 6.4 keV with an equivalent width measured by ASCA of 107^{+42}_{-37} eV (R00). The BeppoSAX observation gives a more poorly constrained value for the EW of 85 ± 65 eV. Furthermore, following R00, a broad iron line with an $\text{EW} < 200\text{--}300$ eV may still be consistent with the ASCA data. On the other hand, the bad signal to noise above 10–20 keV has prevented any good detection of a possible reflection component.

NGC 4258 is well known for the detection, from high resolution observations, of a water maser. It is expected to be produced by the accreting gas spiraling down to the central engine (Claussen, Heiligman & Lo 1984; Watson & Wallin 1994; Miyoshi et al. 1995). The combination of the central mass estimate (deduced from the water maser properties, Heernstein et al. 1999; Miyoshi et al. 1995), and the NIR-to-X-ray luminosity suggest that NGC 4258 is an AGN in a low state with an Eddington accretion rate of 0.0002 (F01). The presence of an ADAF seems however to be ruled out by the recent BeppoSAX observations, on the base of both the measured X-ray spectral shape and X-ray variability, and the most natural explanation of the X-ray luminosity of this source may be in terms of Comptonization of soft photons in a hot corona (F01). The inclination of the disk is large and very well constrained $i=82 \pm 1$ degrees (Herrnstein et al. 1999). We thus expect the Comptonization effects on the reflection components coming from the disk to be relatively important, especially in the case of a slab corona.

We can thus wonder, from the results obtained in the previous sections, what constraints we can put on the origin of the reflection features detected in this object. To this purpose, we have first try to estimate the physical parameters (mainly the temperature and optical depth) of the the corona. We have thus fit the BeppoSAX data (downloaded from the BeppoSAX archive) with H94, assuming an inclination angle of $= 82^\circ$ (i.e. $\mu = 0.14$). Since the intensity of the hard component is strongly reduced by photoelectric absorption below 2–3 keV, we only fit the data above 2.5 keV. Due to the low signal-to-noise ratio of the spectrum, especially at high energy, and the lack of data to constrain the soft photon temperature kT_{bb} , τ and kT_e are badly constrained, τ being smaller than 1 at the 90% confidence level for 2 parameters, with a best fit value of 0.05.

These large uncertainties still enable us to make some interesting comments. First, let us assume, as considered by R00, that the narrow iron line observed in NGC 4258 is from the accretion disk. Then it has to originate at relatively large radii ($R_e > 100$ Schwarzschild radii) in order to produce the observed small line width. In this case, and since the inclination angle of the disk is large (we assume that the inclination of the inner part of the disk is also of 82° , i.e. the disk is not strongly warped) we expect part of the iron line photons to be comptonized in the corona. Thus, as shown in section 4, the EW may be significantly reduced in comparison to the one we expect without a comptonizing corona. Let us suppose that all iron line photons have to cross the corona before being observed (this would be the case if the coronal

dimension D is large i.e. $D > R_e$ as underlined by R00). The observed EW of 100 eV would then correspond to an actual uncomptonized face-on line EW (the $\text{EW}_{\text{dir}}(\mu = 1)$ parameter in Eq. (3)) larger than 300 eV (~ 500 eV for $\tau = 0.05$ and ~ 40 keV for $\tau = 0.5$!). Recent estimates of the average narrow iron line equivalent width observed in Seyfert 1 galaxies rather suggest a value of the order ~ 100 eV (Matt 2000; Lubinski & Zdziarski 2000). This would corresponds to an $\text{EW}_{\text{dir}}(\mu = 1)$ of ~ 200 eV for $\tau = 0.5$ and a viewing angle of 30° (as estimated by Nandra et al. 1997 for Seyfert 1). These (admittedly qualitative) computations rather suggest that the narrow iron line in NGC 4258 does not suffer Comptonization. The most simple explanation, with the assumption that the X-ray emitting region has a disk–corona configuration, is that the narrow iron line preferentially originates from matter not associated with the accretion disk.

In this case, and following R00, we can also set an upper limit on the equivalent width of the uncomptonized broad iron line consistent with its non detection by ASCA. R00 have estimated that the corresponding face-on EW of a possible broad line has to be smaller than $\sim 200\text{--}300$ eV to be consistent with the data. This estimate takes into account the limb darkening and relativistic bending effects but not the Comptonization of the iron line photons in the corona. If such an effect is also taken into account (and still assuming an inclination of 82°), the limits are less strict and a broad line with a face-on uncomptonized $\text{EW} \sim 0.8\text{--}1.2$ keV (for $\tau \sim 0.05\text{--}0.1$) would still be consistent with the ASCA data. Then if there were a broad line present at the level seen in most other AGN ($\sim 100\text{--}300$ eV, Nandra et al. 1997; Lubinski & Zdziarski 2000), we do not expect to see it. The data thus do not require that the inner part of the accretion disc be truncated as suggested in R00.

6.2 Correlations between reflection features and X-ray slope

The Comptonization effects we have discussed so far may influence the apparent correlation we observe between the reflection features characteristics (broad Fe line EW, reflection normalization) and the other parameters of the high energy continuum.

In a recent paper LZ00 have analyzed the complete available ASCA database to re-examine the issue of the strength and width of the Fe $\text{K}\alpha$ line in Seyfert galaxies. An interesting results they report is an apparent correlation between the broad iron line EW and the spectral index in this class of objects. The correlation is actually observed in the average spectra of Seyferts galaxies grouped according to their spectral hardness. As underlined by the authors, this correlation may be naturally explained in the framework of thermal Comptonization model. Indeed, in this case, the power law slope of the X-ray/ γ -ray spectrum emitted by the hot comptonizing corona is related to the rate of cooling by incident soft photons. Then the spectral slope will be correlated with the broad line EW, provided that the main source of the cooling photons is emitted by the same medium that is responsible for the observed reflection features. Furthermore, this interpretation is consistent with

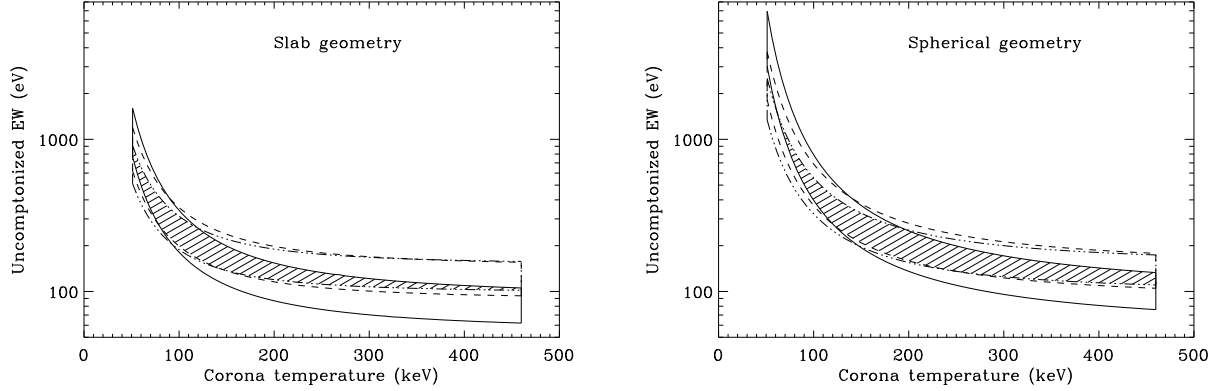


Figure 8. The solid, dashed and dotted-dashed lines are the 90% envelopes of the uncomptonized iron line EW computed for the three spectral indexes reported by LZ00, i.e. $\Gamma = 1.62, 1.82$ and 1.94 respectively. The hatched area correspond to the intersection of the three envelopes. For any fixed value of $EW_{\text{dir}} \gtrsim 100$ eV, this area delimits the range of acceptable common values of the coronal temperature in the three samples. Alternatively, for any fixed value of kT_e , the hatched area corresponds to the acceptable range for the broad line equivalent widths. The left and right plots show the case of a slab and spherical geometry respectively.

the Γ - R correlation observed by Zdziarski et al. (1999) in a sample of Seyfert and galactic black hole candidates (see also Gilfanov et al. 1999; Matt 2000).

We show here that the Comptonization effects in coronae of different intrinsic properties (i.e. different temperature and optical depth) between different objects may also contribute to produce this kind of correlation.

In thermal Comptonization theory, τ and kT_e are related to the X-ray spectra photon index Γ through the approximate relation (Osterbrock 1974; Pozdniakov, Sobol & Siuniaev 1976; Zdziarski 1985):

$$\Gamma = -\frac{\ln P_{\text{sc}}}{\ln A}. \quad (4)$$

In this equation, P_{sc} is the average scattering probability, its expression depending on the coronal geometry, and $A = 1 + 4 \frac{kT_e}{m_e c^2} + 16 \left(\frac{kT_e}{m_e c^2} \right)^2$ is the average photon energy amplification per scattering. In the following, we only treat the cases of slab and spherical geometry. The expression of P_{sc} in these cases can be found in Zdziarski et al. (1994) and Wardzinski & Zdziarski (2000) respectively.

For a given value of the photon index, we can then use Eq. (4) to compute the optical depth τ for different values of kT_e . Assuming that the broad iron lines observed by LZ00 have been comptonized in the corona, we can then compute the EW of these lines before Comptonization, EW_{dir} , by inverting Eq. 3 (we fix the inclination angle to 45 degrees, which is the best fit value obtained by LZ00). In Fig. 8a and 8b (corresponding to a slab and a spherical geometry, respectively) we have plotted the 90% confidence envelopes for EW_{dir} and kT_e obtained for each of the three average values of the spectral indexes reported by LZ00, i.e. $\Gamma = 1.62, 1.82$ and 1.94 . These envelopes have been computed by taking into account the 90% errors of the photon index and of the observed EW reported by LZ00. The solid, dashed and dotted-dashed envelopes in these figures correspond to $\Gamma = 1.62, 1.82$ and 1.94 , respectively. The hatched surfaces correspond to the region of the parameter space where the

EW_{dir} computed for the different photon index classes are equal within the errors.

Interestingly, the values of EW_{dir} are consistent with each other (within the errors) for a relatively large range of coronal temperatures and optical depths, particularly for the spherical geometry where $EW_{\text{dir}} \simeq 100\text{--}150$ eV for $kT_e \gtrsim 150$ keV and $\tau \lesssim 0.6$. In the slab case, $EW_{\text{dir}} \simeq 100\text{--}150$ eV for $100 \lesssim kT_e \lesssim 250$ keV and $0.6 \gtrsim \tau \gtrsim 0.1$. These results thus show that the presence in different objects, all having broad lines with similar EW (before Comptonization), of hot coronae with different physical characteristics (i.e. different τ and kT_e), may result in an apparent EW - Γ correlation (as the one observed by LZ00).

It is worth noting that the main implication of this interpretation is that the coronae producing the harder spectra (smaller Γ) must also have the larger optical depth. Such behaviour *necessarily goes with a change of the Compton parameter* (i.e. a change of the geometrical and/or energetical properties of the corona) since for constant y a correlation between τ and Γ is expected (Haardt et al. 1997).

We note that, in this picture, we also expect a correlation between the observed reflection normalization R and the photon index Γ . Indeed, as shown in section 5, for larger optical depth the Comptonization effects smooth the reflection hump so that fitting with an uncomptonized reflection gives smaller R . This goes in the sense of the results of Z99, although, as shown in section 5, we do not expect strong effects ($\lesssim 30\%$ for inclination angles smaller than 60°) on the reflection normalization.

A possible reason for an anticorrelation between τ and Γ may be the following. Suppose that the corona+disk configuration is the one proposed by Z99 i.e. a central hot plasma + cold disc model, the inner radius of the disk being able to vary. In this interpretation, the increase of the inner radius of the disk, which will produce a decrease of R and Γ , may be due to the evaporation of part of the inner re-

gions of the disk (due to some disk instabilities, Meyer et al. 2000; Menou et al. 2000; Turolla & Dullemond 2000) in the corona, thus resulting in an increase of the corona optical depth. Interestingly, in this case, the comptonization effects would reduce the apparent reflection component and thus could explain the small R values observed at small Γ , emphasizing the strength of the observed correlation.

In conclusion, the main point of this section is that, due to likely different corona characteristics from one object to the other, the comptonization effects may have some influence to produce and/or emphasize the observed correlations between the reflection features and X-ray slope.

6.3 Consequences for the X-ray background

After the most recent surveys (Mushotzky et al. 2000; Hasinger et al. 2001) there is now a tantalizing evidence that the X-ray Background (XRB) is mainly due to the integrated emission of single sources, i.e. AGNs lying at cosmological distances. All the spectral models for the XRB assume that the intrinsic AGN spectrum (before any absorption in a putative large scale molecular torus) is the sum of a power-law continuum and an uncomptonized reflection. We expect that the effects described here can be of some relevance for any detailed fitting model for the XRB. In Fig. 9 we show, as an illustrative case, an angle averaged reflection hump calculated for $kT_e = 90\text{keV}$ and $\tau = 0.35$ (corresponding to $y = 0.6$) for both the comptonized (solid line) and uncomptonized (dashed line) case. Indeed, in all current models (Madau, Ghisellini & Fabian 1994; Wilman & Fabian 1999; Gilli, Salvati & Hasinger 2001), for an average continuum slope of about 2, the peak of the XRB (in νF_ν) is associated with the peak of the reflection hump. Furthermore, there is evidence that the observed peak of the X-ray background is located at slightly higher energies than those predicted by the standard models that neglect the effect of Comptonization in the corona.

Although many uncertainties come into the exact determination of the possible consequences of such effect on the XRB shape, as the temperature and optical depth distribution in the different sources or the total coronal covering fraction, the work we have presented here should indicate that Comptonization of the reflection component in the corona have to be taken into account when dealing with accurate spectral fitting of the X-ray background.

7 CONCLUSION

In this paper, we have shown that the effects of a comptonizing corona on the appearance of the reflection components can be relatively important, modifying the shape of the reflection hump and the iron line equivalent width measurements. We have studied in detail the dependence of these effects on the physical (i.e. the temperature kT_e and optical depth τ) and geometrical (i.e. the inclination angle) parameters of the corona, mainly focusing on the case of a slab geometry. This is an extreme case since the corona covers all the reflecting material and consequently the comp-

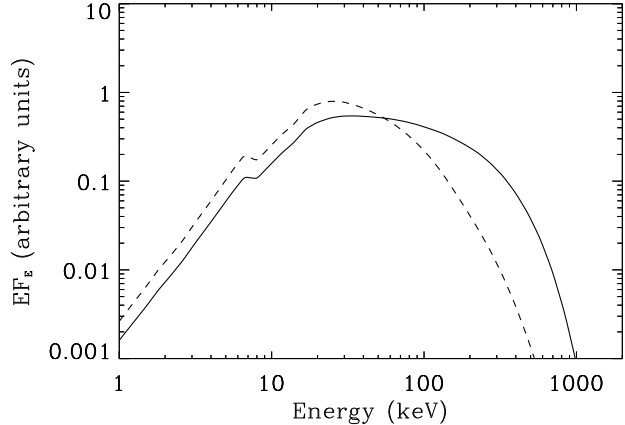


Figure 9. An angle-averaged reflection hump calculated for $kT_e = 90\text{keV}$ and $\tau = 0.35$ (corresponding to $y = 0.6$). The solid line represents the comptonized reflection, the dashed the direct one. The slight shift of the peak energy of the hump is an indication of the predicted effect of the Comptonizing corona on the location of the peak energy in the X-ray background.

tonization effects are large. The results of this study can be summarized as follows:

- Due to the smoothing and shifting towards high energies of the comptonized reflection hump, the main effects on the emerging spectra appear at energies below and above $\sim kT_e$.
- They are larger for larger optical depth of the corona and/or larger inclination angle of the corona-disk configuration.
- Fitting Comptonization models taking into account comptonized reflection by the usual cut-off power law + uncomptonized reflection models, leads to an underestimation of the reflection normalization and an overestimation of the high energy cut-off.
- The Comptonization effects may strongly reduce the equivalent width of the observed iron line, especially at large inclination angles.

These effects may have important consequences on the physical interpretation of the presence and/or absence of reflection features in astrophysical objects. As an example, we have studied the case of the galaxy NGC 4258. With the assumption that the X-ray emitting region has a disk-corona configuration and given the high inclination angle of the accretion disk in this source, the comptonization effects enable to find less strict limits on the EW of a possible broad Iron line, then explaining its non-detection. Besides, in this picture, the narrow iron line observed in this object is believed to originate preferentially from matter not associated with the accretion disk since, in the contrary case, it would require a primary (i.e. before Comptonization) iron line with a (unlikely) too large EW.

We also find that the presence of a comptonizing corona can produce and/or emphasize the correlations between the reflection features (like the iron line equivalent width or the covering fraction) and the X-ray spectral index. Then, similarly to the effects produced by a bad modelisation of the complex ionization pattern expected at the surface of the X-

ray-irradiated reflecting material, these different effects are to be properly taken into account to correctly interpretate these correlations.

Finally, we underline the possible importance of the Comptonization effects on the reflection shape when dealing with accurate spectral fitting of the X-ray background. Indeed, there is evidence that the observed peak of the X-ray background is located at slightly higher energies than those predicted by the standard models that neglect the effect of Comptonization in the corona.

ACKNOWLEDGMENTS

We are grateful to the referee, Chris Done, for the careful revision of the paper and her valuable comments and suggestions. POP acknowledges a grant of the European Commission under contract number ERBFMRX-CT98-0195 (TMR network "Accretion onto black holes, compact stars and protostars"). We thank J. Malzac for useful suggestions. We also thank F. Fiore for having given to us the draft on NGC 4258 in advance of publication.

REFERENCES

Bai, T. & Ramaty, R. 1978, *ApJ*, 219, 705
 Ballantyne, D. R., Ross, R. R., & Fabian, A. C. 2000, *MNRAS* in press (astro-ph/0102040)
 Beloborodov, A. M. 1999, *ApJ Letter*, 510, L123
 Claussen, M. J., Heiligman, G. M., & Lo, K. Y. 1984, *Nature*, 310, 298
 Done, C. & Nayakshin, S. 2001, *ApJ*, 546, 419
 Fabian, A. C., Iwasawa, K., Reynolds, C. S., & Young, A. J. 2000, *PASP*, 112, 1145
 Fiore F., Pellegrini S., Matt G. et al. 2001, *ApJ* in press (astro-ph/0102438) (F01)
 George, I. M. & Fabian, A. C. 1991, *MNRAS*, 249, 352
 Ghisellini, G., Haardt, F. & Matt, G. 1994, *ApJ Letter*, 429, L53
 Gierlinski M., Zdziarski A. A., Done C. et al. 1997, *MNRAS*, 288, 958
 Gilfanov, M., Churazov, E., & Revnivtsev, M. 1999, *A&A*, 352, 182
 Gilli, R., Salvati, M., & Hasinger, G. 2001, *A&A*, 366, 407
 Haardt, F. & Maraschi, L. 1991, *ApJ Letter*, 380, L51
 Haardt, F. & Maraschi, L. 1993, *ApJ*, 413, 507
 Haardt, F., Done, C., Matt, G., & Fabian, A. C. 1993, *ApJ Letter*, 411, L95
 Haardt, F. 1994, PhD dissertation, SISSA, Trieste (H94)
 Haardt, F. , Maraschi, L. & Ghisellini, G. 1997, *ApJ*, 476, 620
 Herrnstein, J. R. et al. 1999, *Nature*, 400, 539
 Hua, X. & Lingenfelter, R. E. 1992, *ApJ*, 397, 591
 Lightman, A. P. & White, T. R. 1988, *ApJ*, 335, 57
 Lubinski, P. and Zdziarski, A. A. 2000, submitted to *MNRAS* (astro-ph/0009017) (LZ00)
 Madau, P., Ghisellini, G., & Fabian, A. C. 1994, *MNRAS*, 270, L17
 Magdziarz, P. & Zdziarski, A. A. 1995, *MNRAS*, 273, 837
 Malzac J., Beloborodov, A. & Poutanen, J. *MNRAS* in press (astro-ph/0102490)
 Matsuoka, M., Piro, L., Yamauchi, M. & Murakami, T. 1990, *ApJ*, 361, 440
 Matt, G., Perola, G. C. & Piro, L. 1991, *A&A*, 247, 25
 Matt, G., Fabian, A. C., & Reynolds, C. S. 1997, *MNRAS*, 289, 175
 Matt, G., to appear in the proceedings of "X-Ray Astronomy '99", 1999, September 6-10, Bologna (Italy), (M00, astro-ph/0007105)
 Menou, K., Hameury, J., Lasota, J., & Narayan, R. 2000, *MNRAS*, 314, 498
 Meyer, F., Liu, B. F., & Meyer-Hofmeister, E. 2000, *A&A*, 361, 175
 Miyoshi, M., Moran, J., Herrnstein, J., Greenhill, L., Nakai, N., Diamond, P., & Inoue, M. 1995, *Nature*, 373, 127
 Nandra, K. & Pounds, K. A. 1994, *MNRAS*, 268, 405
 Nandra, K., George, I. M., Mushotzky, R. F., Turner, T. J., & Yaqoob, T. 1997, *ApJ*, 477, 602
 Narayan, R., Mahadevan, R. & Quataert, E. 1999, *Theory of Black Hole Accretion Disks*, 148, Cambridge University Press, Cambridge
 Osterbrock, D. E. 1974, *Astrophysics of gaseous nebulae*, W. H. Freeman and Co., 1974. 263 p.,
 Petrucci, P. O. et al. 2000, *ApJ*, 540, 131
 Pounds, K. A., Nandra, K., Stewart, G. C., George, I. M. and Fabian, A. C. 1990, *Nature*, 344, 132
 Pozdniakov, L. A., Sobol, I. M. & Siuniaev, R. A. 1976, *Soviet Astronomy Letters*, 2, 55
 Reynolds, C. S. & Fabian, A. C. 1997, *MNRAS*, 290, L1
 Reynolds, C. S., Nowak, M. A., & Maloney, P. R. 2000, *ApJ*, 540, 143 (R00)
 Stern, B. E., Begelman, M. C., Sikora, M. & Svensson, R. 1995, *MNRAS*, 272, 291
 Svensson, R. 1996, *A&ASS*, 120, C475
 Turolla, R. & Dullemond, C. P. 2000, *ApJ Letter*, 531, L49
 Wardziński, G. & Zdziarski, A. A. 2000, *MNRAS*, 314, 183
 Watson, W. D. & Wallin, B. K. 1994, *ApJ Letter*, 432, L35
 White, T. R., Lightman, A. P. & Zdziarski, A. A. 1988, *ApJ*, 331, 939
 Wilman, R. J. & Fabian, A. C. 1999, *MNRAS*, 309, 862
 Zdziarski, A. A. 1985, *ApJ*, 289, 514
 Zdziarski, A. A., Fabian, A. C., Nandra, K., Celotti, A., Rees, M. J., Done, C., Coppi, P. S., & Madejski, G. M. 1994, *MNRAS*, 269, L55
 Zdziarski, A. A., Lubinski, P. and Smith, D. A. 1999, *MNRAS*, 303, L11 (Z99)